GEOMATICS AND ENVIRONMENTAL ENGINEERING • Volume 18 • Number 6 • 2024

https://doi.org/10.7494/geom.2024.18.6.23

Sudhir K. Powar[1], Sachin S. Panhalkar[2]

Flood-susceptibility Analysis of Kolhapur City Using Frequency Ratio Model

Abstract: Flooding is an inevitable but natural process that happens over the period of time; it not only endangers people's health, wealth, and assets, but it has also a negative impact on a country's economy. Hence, effective flood management is required in order to minimize the influence of flooding on human lives and livelihoods. The aim of this research is to use a frequency ratio model (FRM) to identify flood-susceptibility areas in the city of Kolhapur. The research was conducted in two parts. Initially, field-survey data was used to create a flood-inventory map. There were 255 flood locations identified throughout the research region; of these, 178 locations (70%) were used for training data, and 77 (30%) were used for verification purposes. The spatial database was then used; from this, ten flood contributing parameters were generated: slope, elevation, rainfall, distance from a river, a stream power index (SPI), a topographical wetness index (TWI), a topographical roughness index (TRI), a plan curvature and profile curvature, and land use/land cover. Finally, an FR model database was created for flood-susceptible mapping. The prepared database was separated into four flood-susceptibility zones: low susceptibility, medium susceptibility, high susceptibility, and very high susceptibility. About 26.08% of the land was classified as 'very high susceptibility,' while 21.18% was classified as 'high susceptibility.' The final flood-susceptibility map was verified by using the receiver operating characteristic (ROC) curve. The results indicated that the method that was used in this study provided accurate results (with a success rate of 87%); this indicated an acceptable result for our flood-susceptibility zonation. Local administrations, researchers, and planners will benefit greatly from this flood-susceptibility analysis in developing flood-prevention plans.

Keywords: flood susceptibility, frequency ratio model, receiver operating characteristic curve, geographic information system

Received: February 28, 2024; accepted: September 29, 2024

[1] Shivaji University, Department of Geography, Kolhapur, Maharashtra, India, email: sudhirpowar100@gmail.com (corresponding author), https://orcid.org/0000-0003-4591-3084

[2] Shivaji University, Department of Geography, Kolhapur, Maharashtra, India, email: panhalkarsachin@gmail.com

1. Introduction

Every year, a significant number of people lose their lives and experience extensive damage to their properties due to both natural and human-induced calamities such as floods, earthquakes, and landslides [1, 2]. Among these, flooding is considered to be one of the most hazardous hydro-meteorological threats worldwide [3–5]. Flooding poses a grave risk to human lives and causes substantial socio-economic devastation [6, 7]. According to the United Nations, there were approximately 150,061 flood events globally between 1995 and 2015; these resulted in around 157,000 deaths and accounted for 11.1% of the total number of fatalities that were caused by natural disasters [8]. According to the Central Water Commission (CWC), India ranks as the world's second-most-flood-prone country (trailing only Bangladesh). Approximately 40 million hectares of land in India are at risk of flooding. Each year, an average of 7.6 million hectares of land in India are affected by floods. The devastating impact of floods in India is evident from the estimated capital damages of about $200 billion and the losses of 92,000 lives between 1953 and 2009 (as reported by the CWC). Considering that India accounts for nearly 20% of the world's population, the annual loss of life due to floods is significant. During the rainy season in India, floods claim the lives of approximately 1,500 people, affecting around 30 million individuals on average [9–11]. The scale of the devastation that is caused by flooding highlights the urgent need for effective measures to mitigate and manage this calamity in the country.

Even though flooding is a severe natural calamity, preventing it is practically impossible [12]; thus, flood-susceptibility mapping and flood-vulnerability assessments are required in order to construct management systems for minimizing flood vandalism in the future; they are valuable tools for guiding administrations and planners to develop suitable flood-management policies [13–15]. Furthermore, flooding occurrence rates and frequencies are expected to worsen by 2050 based on variations in the climate, changes in land use, and population growth; this will potentially result in a $10 billion loss [16, 17, 19–21]. As a result, studies on substantially happening flood modeling at the watershed and regional levels is critically needed for flood-prevention measures [6, 21, 22].

Over the past few decades, the utilization of remote sensing (RS) and geographic information systems (GIS) has gained significant popularity. These technologies offer new dimensions to vulnerability analysis and justification by providing precise information about a region. The analysis of satellite images on RS and GIS platforms has yielded promising results in the development of flood-susceptibility and flood-risk maps [23, 24]. The integration of RS and GIS creates an ideal environment in which various models can be employed and data can be manipulated in order to estimate flood susceptibility. This approach leads to more-accurate and more-meaningful results. Consequently, these techniques are being successfully implemented worldwide to assess flood susceptibility [13, 25–27].

Flood-susceptibility analysis involves assessing the likelihood of an area being affected by floods. In effect, selecting the essential elements for flood-susceptibility assessments is fundamentally crucial in order to obtain accurate results; even if one flood-reducing element might be particularly effective in a given area, it might not be in other places [14, 28]. There are many causative elements that can effect on flood susceptibility; namely, slope and a topographic weightiness index (TWI) (which shows the areas and local slope-based hydrologic behaviors of watersheds). Therefore, a digital elevation model (DEM) grid cell's risk of accumulating water (inundation) increases with increasing TWI values [29]. A topographic roughness index (TRI) is a useful element in flood-susceptibility mapping; it provides measurements of the variations in elevation or terrain ruggedness within a given area (which can influence the flow of water during flood events) [13]. In the current research, the methodology incorporates ten conditioning elements (which are thoroughly elucidated in the methodological section). These elements have been carefully selected to ensure a comprehensive and robust analysis.

Flood-susceptibility and flood-vulnerability mapping can also be done by using a different models and techniques. One of the most extensively used and reliable methodologies for susceptibility assessment is the frequency ratio (FR) method [30]; this is a sort of statistical approach wherein each parameter's class is given a quantitative score, and its effect on the probability of flooding is evaluated [31, 32]. The FRM is grounded in the principle of uniformitarianism, which holds that historical events, such as floods or landslides, are likely to recur in similar ways. FR analysis applies a binomial statistical approach, allowing precise correlation analysis between two variables – typically, one dependent and the other independent [33]. This establishes a mathematical relationship between flood frequency and relevant conditioning factors [15]. An FR value below 1 indicates a weaker relationship, whereas a value above 1 reflects a stronger correlation [30, 34]. Beyond assessing the correlation between conditioning factors and flood occurrences, FRM facilitates the calculation of a flood susceptibility index, aiding in the development of flood-hazard maps. Consequently, FR, as a data-driven tool, is invaluable for analyzing the correlation between flood events and conditioning factors, as well as for effective hazard mapping. This model works in a GIS-based environment and can generate scientifically accurate flood-susceptibility maps [35, 36]. Its advanced tools (like remote sensing and GIS) provide straightforward ways of making flood-susceptibility maps using the FR model.

Kolhapur and its surrounding villages have been subjected to Panchaganga River floods on a regular basis over the past three decades – particularly during each monsoon season. The flood of 2005 took the entire city by unpleasant surprise. Being the first flood that was faced after ages, it was quite difficult to cope with back then; it took time to overcome its effects. However, the city was again hit by floods in 2019 and 2021, leading to huge losses of human lives and properties. This gave rise to the need to study the floods as well as their causes and consequences; thus, the main objective of this research is to create a flood-susceptibility map for Kolhapur and its surrounding areas.

2. Study Area

The present study region is extended between 16° 37′ and 16° 48′ N latitudes and 74° 10′ and 74° 18′ E longitudes which is shown in Figure 1. The study covers a total area of 185.69 km^2. Kolhapur and its neighboring suburbs are included. The Panchaganga River, a tributary of the Krishna, flows through the study region (mostly on the northern side). The study region is 546 meters above sea level (m a.s.l.) and has a mild climate, with a minimum temperature of 15°C, a maximum temperature of 40°C, and an average annual rainfall of 1,043 mm.

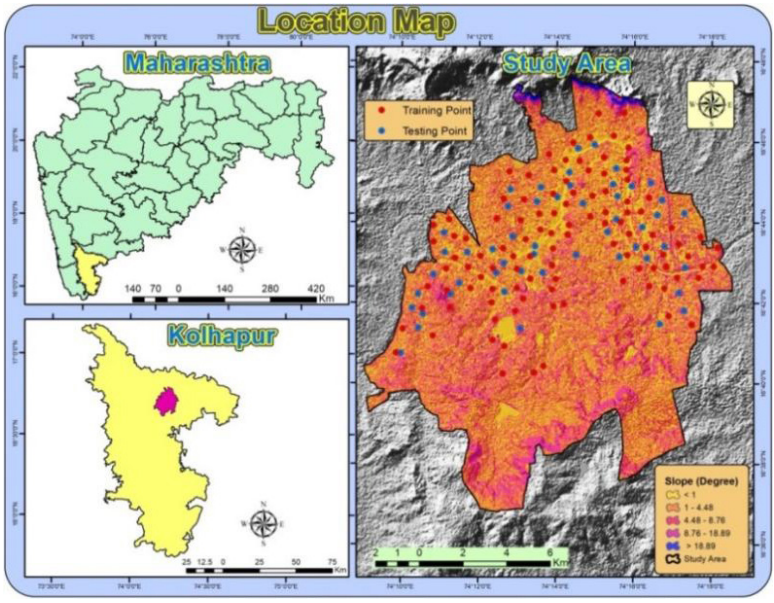

Fig. 1. Study area location map with flood points

3. Database and Methodology

In the process of flood-susceptibility mapping for Kolhapur, ten different factors were selected and integrated using an ArcGIS environment. Table 1 provides the detailed specifications and features of the various data sets that were involved. The CartoDEM data was utilized to generate a slope map as well as elevation, TWI, SPI, a plan curvature, a profile curvature, and a drainage-proximity map (Table 1). The Resourcesat LISS-IV image was employed to create the land use/land cover (LULC) data, while the Maharain data was utilized to prepare the rainfall map. The methodology for generating the flood-susceptibility map can be referred to in Figure 2.

Table 1. Detailed database that was used for research

Description of data	Format and resolution of data	Year of data	Data source
Resourcesat LISS-IV	satellite image, 5.8 m	2021	NRSC
CartoDEM	satellite image, 2.5 m	2020	NRSC
Rainfall	point	2013–2020	Maharain.maharashtra.gov.in
Historical flood locations	point	before 2021	satellite image and field investigation

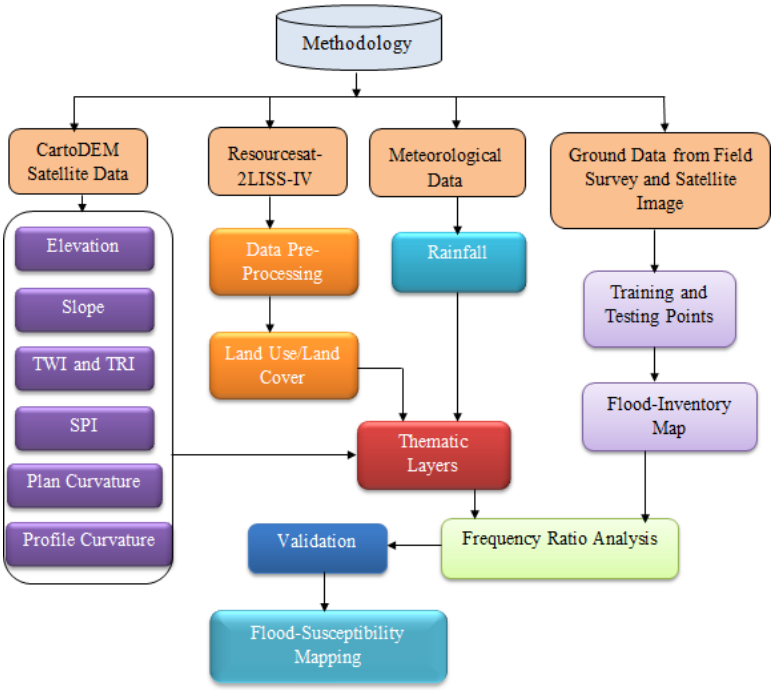

Fig. 2. Research methodology

3.1. Flood-inventory Map

Flood-susceptibility mapping relies heavily on scientifically confirmed flood-occurrence data from the past, as this plays a crucial role in estimating future flood susceptibility and any associated risks [37]. The availability and analysis of flood-inventory information are essential components in this process. By studying past flood events, researchers can gain valuable insights into the factors that contribute to the flood susceptibility in a given area. This study employed two techniques to collect flood-location data: the DGPS instrument (for the field investigation), and radar satellite data (for digitizing some flood locations in the ArcGIS environment). By combining these methods, a flood-inventory map was generated,

which contained 255 flood locations (Fig. 1) for the extreme flood events that occurred in 2019 and 2021. This was randomly separated into two parts of training and validation data sets for preparing and justifying the flood-susceptibility result.

When allocating flood points to the training and testing data, there was no set of standards [38]. The majority of the research was done using 70% of the flood points as training data for creating the flood-susceptibility models and 30% as validation data for the output model [39, 40]. In this work, 70% of the training points were chosen at random for the flood modeling, and 30% of the verification points were chosen at random for model verification [33].

3.2. Flood-conditioning Factors

The incidence of floods in a specific location is influenced by a variety of environmental and human-made elements. As a result, selecting essential elements for a flood-susceptibility assessment is fundamentally crucial in order to obtain an accurate result; even though one flood-reducing element might be particularly effective in a given area, it might not necessarily work in other places [14, 28]. For the current research, ten conditioning elements were taken into account: slope, elevation, rainfall, river proximity, SPI, TWI, TRI, profile curvature, plan curvature, and LULC. These ten parameters were chosen because they are important factors that influence floods in particular areas. The importance of each parameter is explained separately below.

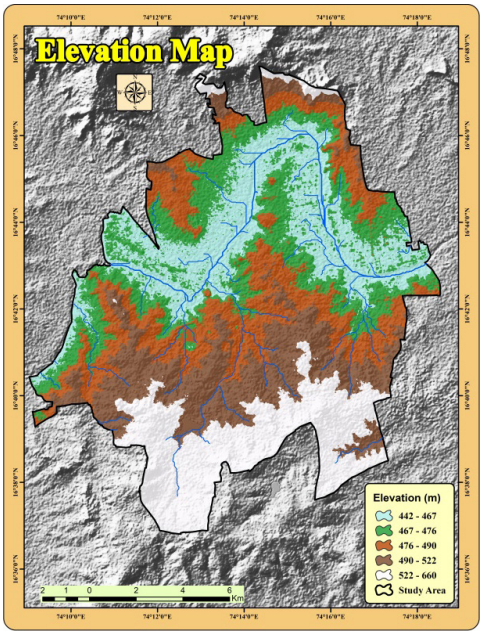

Fig. 3. Elevation map

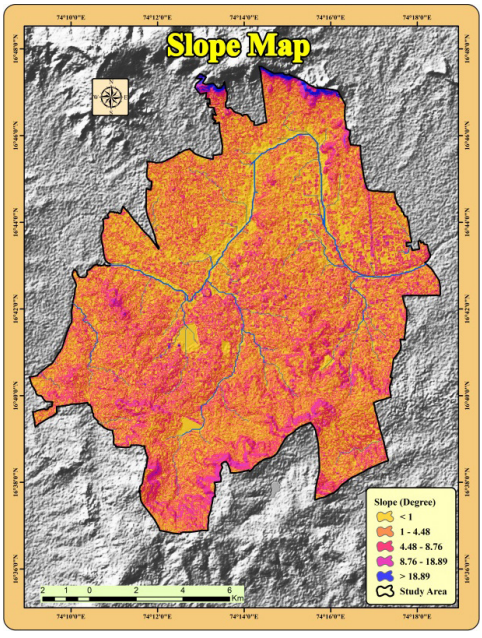

Fig. 4. Slope map

In flood-susceptibility mapping, elevation and slope are essential elements, and variations in elevation have an impact on climate features [41]. Surface runoff and vertical percolation can be controlled by an area's slope [42]. Thus, the study area's slope and elevation maps were prepared from the CartoDEM image using ArcGIS software (Figs. 3, 4).

Flood susceptibility can be influenced differently by various types of LULCs in a location. Forest cover has a detrimental impact on flooding because it promotes infiltration, which slows water runoff and recharges the subsurface [33, 43, 44]; on the other hand, built-up areas with a lot of surface run-off contribute to flooding. Thus, an LULC database was prepared using Recourse Sat-2 LISS-IV data using the object-based classification technique (Fig. 5). Flooding and heavy rainfall have a positive relationship, because surface runoff during heavy rains is a significant factor for predicting floods. The study area's rainfall map was created using the interpolation method (Fig. 6).

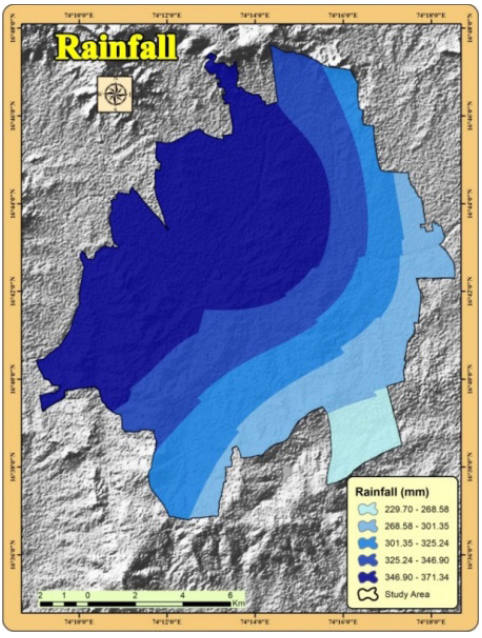

Fig. 5. LULC map

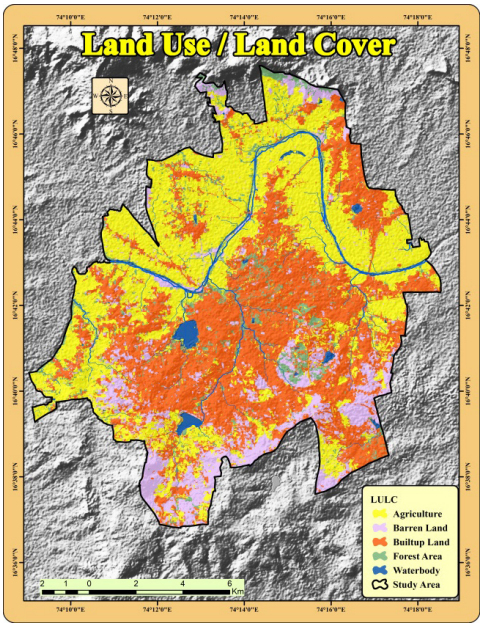

Fig. 6. Rainfall map

Flooding usually occurs near a river's bank and in low-lying flood plain areas. The intensity of a flood is influenced by the proximity of a river; thus, river proximity (or the distance from the main river) was one important element that was established through proximity analysis in ArcGIS (Fig. 7). SPI is often employed as a flood-conditioning factor; it calculates the erosive potential of runoff and maintains terrain stability [13]. SPI shows where soil-conservation efforts have minimized the

erosive effects of surface runoff [45]. An SPI map of the study region (Fig. 8) was extracted as a secondary derivative of DEM as per Equation (1) and divided into five groups using the spatial analyst tools in ArcGIS:

$$SPI = \alpha \tan\beta \tag{1}$$

where α indicates the catchment area [m^2], and β represents the slope angle [°].

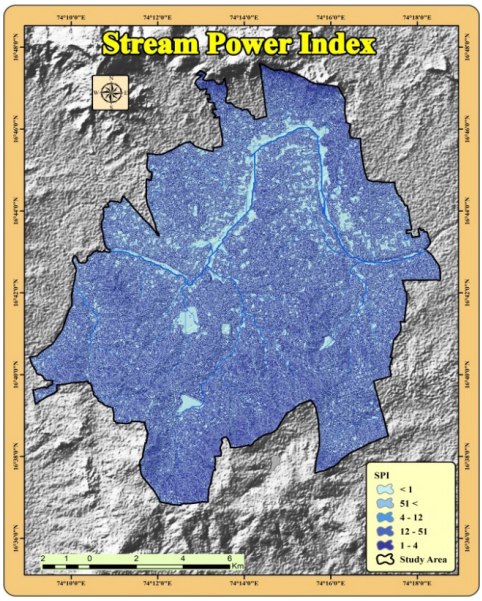

Fig. 7. River proximity map

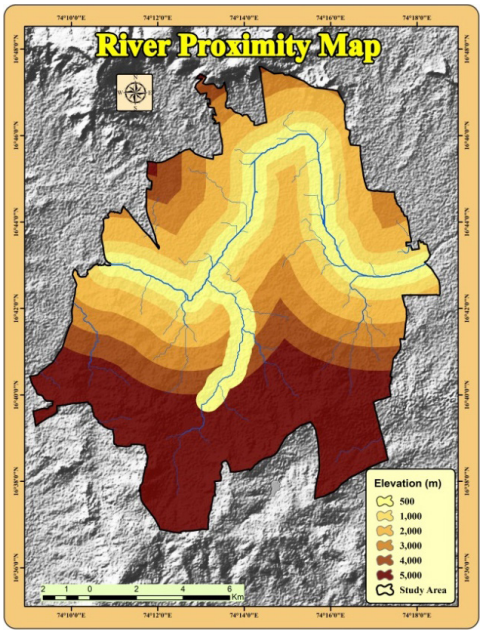

Fig. 8. SPI map

In a floodplain, roughness components like surface variations and inequalities along with vegetation features like plants, shrubs, woods, and stumps can be noticed [46]. A topographical roughness index (TRI) assumes a fundamental value when modeling a flood plain's hydrology [47]. The variations in elevation among the pixel of a DEM are represented by TRI, which is derived using Equation (2). The TRI map of the study region (Fig. 9) was derived using CartoDEM with a 2.5-metre resolution:

$$TRI = \gamma\left[\sum(x_{ij} - x_{00})2\right] \cdot \frac{1}{2} \tag{2}$$

where x_{ij} is the elevation of each nearby cell as compared to a certain cell (0, 0).

TWI shows an area and the local slope-based hydrologic behavior of watersheds; therefore, a DEM grid cell's risk of accumulating water (inundation) increases with increasing TWI values [29]. This indicates the water flow under gravity's impact and can be used to calculate the quantity of a flow's accumulation at any site in a catchment region [48]. TWI is an extremely effective method for determining flood probabilities [23, 28, 32, 33, 49]. As is shown in Equation (3), the TWI map of the research region (Fig. 10) was produced in ArcGIS using the map algebra-raster calculator tool and divided into six groups:

$$\mathrm{TWI} = \ln(\alpha - \tan\beta) \cdot \mathrm{TWI} = \frac{\alpha}{\tan\beta} \tag{3}$$

where α indicates the catchment region [m^2], and β denotes the angle of the slope [°].

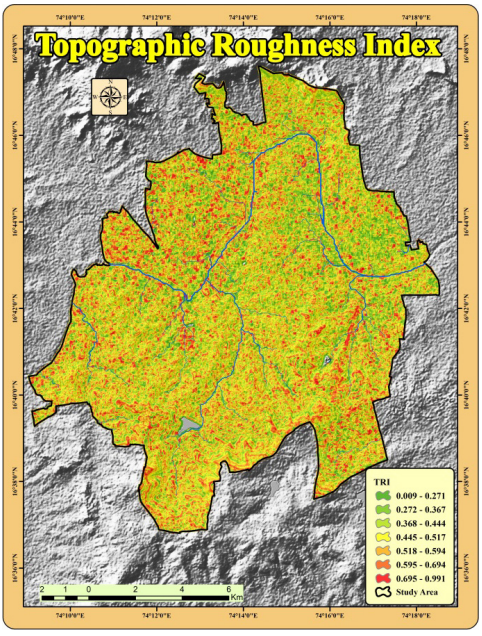

Fig. 9. TRI map

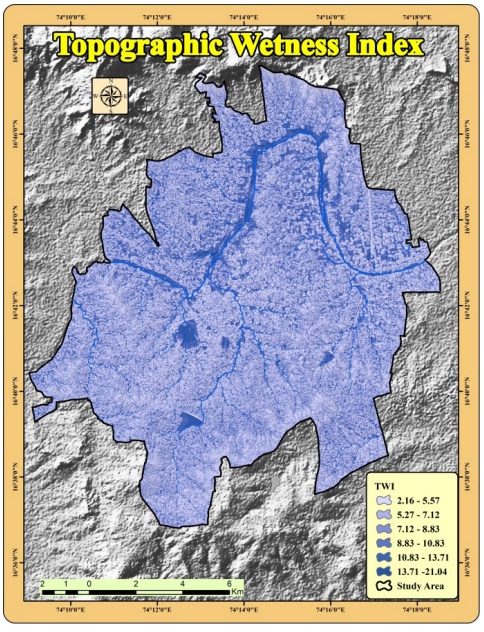

Fig. 10. TWI map

The next important flood-conditioning factor is the profile curvature; this controls the acceleration and deceleration of the surface flow, and it is the curvature of the ground in the orientation of the gradient [50]. Also, erosional and depositional processes are affected by the curvature. The research area's profile-curvature map (Fig. 11) was derived using CartoDEM with a 2.5-metre resolution with use the spatial analyst tools-surface-curvature tool; a negative value represents a convex profile, zero represents a smooth surface, and a positive value denotes concavity in the profile curvature. This was classified accordingly into the three classes.

The next crucial factor is the plan curvature, which refers to the curvature of a surface that is perpendicular to the slope's direction and is connected to a surface flow's convergence and divergence [50]. The research area's plan-curvature map (Fig. 12) was derived using CartoDEM with a 2.5-metre resolution with use the spatial analyst tools-surface-curvature tool; a negative number represents a convex profile, zero represents a smooth surface, and positive denotes concavity in the plan curvature. This value was classified accordingly to the three classes.

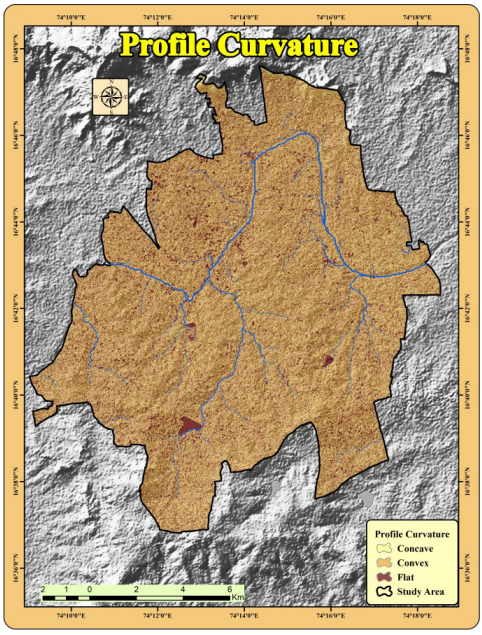

Fig. 11. Profile curvature

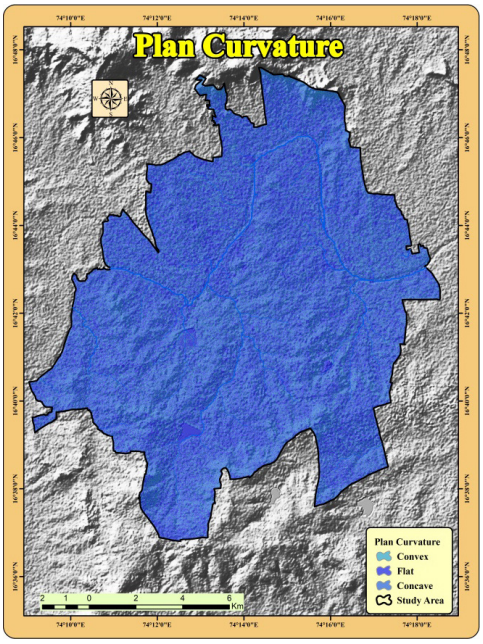

Fig. 12. Plan curvature

3.3. Frequency Ratio Model (FRM)

FRM is based on the uniformitarianism idea that states that a historical event (flood, landslide, etc.) will repeat again in the same manner. FRM is a binomial statistical-analysis method that can be used to precisely find the correlation between two variables: one dependent, and the other independent [33]. This is a mathematical link between flood frequency and a relevant conditioning factor [15]. An FR number that is less than 1 suggests a weaker connection, whereas a value that is greater than 1 indicates a high correlation [34, 51]. Apart from determining the correlation among the conditioning factors and incidents of flooding, FRM also helps to calculate a flood-susceptibility index and, hence, design a flood-hazard map. Accordingly, the frequency ratio model is a data-driven tool that is very useful for calculating the correlations among flood incidents and any flood-conditioning variables as well as for hazard mapping.

Equation (4) was used to determine the final FR values:

$$\mathrm{FR} = f(i) - \Sigma f - p(i) - \Sigma \tag{4}$$

where $f(i)$ denotes the flood cells for each category of the conditioning factors, Σf denotes the number of flood cells in total, $p(i)$ is the number of pixels in each conditioning factor class, and Σp denotes the total number of pixels in the research area. The frequency ratio is the amount of a flooded area in relation to the overall study area with respect to each conditioning factor.

Not only is it a simple approach of analysis, it is a widely employed one as well. The values of the terms that were involved in Equation (4) were derived in the ArcGIS environment. After computing the FR values for each class, each governing factor combined all of the FR values together in order to produce the final output of the flood-susceptibility index (FSI) that is represented in the form of a susceptibility map. Equation (5) was used to generate the flood-susceptibility index:

$$\mathrm{FSI} = \Sigma \mathrm{FR} \tag{5}$$

Finally, the calculated FSI index is reclassified into four flood-susceptibility classes, namely: low, medium, high, and very high susceptibilities.

4. Results and Discussion

There are ten independent variables (known as conditioning factors) that play a role in flood-susceptibility mapping [52, 53]. As a result, spatial extent and statistical information for the ten conditioning factors (namely, slope, elevation, rainfall, river proximity, SPI, TWI, TRI, profile curvature, plan curvature, and LULC) were prepared with their sub-classes (Table 2). The slope of a region determines its flood incidences; for example, simple flat plain regions are highly associated with flooding during rainy seasons because the water cannot drain fast on lower-slope areas. A slope range of 0–8.76° strengthens flooding, as the FR value is significantly close to or greater than one [32]. The slope factor was derived from DEM and classified into five categories. In the present research, the outcome exhibits that the first sub-class of 0–1.5° slopes shows an FR value of more than 1, and the second sub-class of slopes (1.50–4.48°) shows an FR value of 0.77. Nearly 70% of floods happen in locations where the slopes are less than 4.48° (Table 2).

Elevation is one of the most essential flood-control elements. In general, the FR value decreases as the height of a region increases. Table 2 shows that the two lower elevated classes in the study region (442–467 and 467–476 m) had high FR values (3.49 and 1.07, respectively); this indicated that low-elevated areas have significant risks of flooding. Approximately 41% of the total areas in our study were covered by these two sub-classes.

Table 2. Conditioning parameters of flood-susceptibility mapping through FR model

Sr. no.	Description class name	Flood numbers	Percentage of flood numbers [%]	Histogram	Percentage of histogram [%]	FR
Slope [°]						
1	0–1.50	93	52.2471	559,480	30.8070	1.6959
2	1.50–4.48	56	31.4606	739,232	40.7049	0.7728
3	4.48–8.76	24	13.4831	407,049	22.4136	0.6015
4	8.76–18.89	5	2.8089	101,220	5.5735	0.5039
5	18.89–49.68	0	0.0000	9,094	0.5007	0.000
Elevation [m]						
1	442–467	127	71.3483	375,786	20.4380	3.4909
2	467–476	39	21.9101	375,230	20.4078	1.0736
3	476–490	12	6.7415	364,264	19.8114	0.3402
4	490–522	0	0.0000	369,809	20.1129	0.0000
5	522–660	0	0.0000	353,568	19.2296	0.0000
Rainfall [mm]						
1	229.70–268.58	0	0.0000	71,475	3.9192	0.0000
2	268.58–301.35	13	7.3033	251,274	13.7784	0.5300
3	301.35–325.24	9	5.0561	340,752	18.6849	0.2706
4	325.24–346.90	37	20.7865	375,481	20.5892	1.0095
5	346.90–371.34	119	66.8539	784,690	43.0280	1.5537
Distance from river [m]						
1	500	97	54.4943	294,790	16.0394	3.3975
2	1,000	55	30.8988	223,765	12.1750	2.5378
3	2,000	24	13.4831	369,761	20.1186	0.6701
4	3,000	2	1.1235	232,778	12.6653	0.0887
5	4,000	0	0.0000	163,056	8.8718	0.0000
6	5,000	0	0.0000	553,755	30.1296	0.0000
Stream power index						
1	<1	115	64.6067	909,181	50.0629	1.2905
2	1–4	62	34.8314	901,369	49.6328	0.7017
3	4–12	1	0.5617	2,984	0.1643	3.4191
4	12–51	0	0.0000	1,428	0.0786	0.0000
5	51–110	0	0.0000	1,113	0.0612	0.0000

Table 2. cont.

Topographic wetness index						
1	2.16–5.57	41	23.0337	599,145	32.9912	0.6981
2	5.57–7.12	29	16.2921	461,327	25.4024	0.6413
3	7.12–8.83	35	19.6629	335,956	18.4990	1.0629
4	8.83–10.83	49	27.5280	280,061	15.4212	1.7850
5	10.83–13.71	19	10.6741	110,588	6.0893	1.7529
6	13.71–21.04	5	2.8089	28,998	1.5967	1.7592
Topographic roughness index						
1	0.009–0.271	12	6.7415	82,501	4.3924	1.5347
2	0.272–0.367	33	18.5393	246,524	13.1253	1.4124
3	0.368–0.444	38	21.3483	401,525	21.3778	0.9986
4	0.445–0.517	43	24.1573	461,831	24.5886	0.9824
5	0.518–0.594	28	15.7303	380,203	20.2426	0.7770
6	0.595–0.694	18	10.1123	229,716	12.2304	0.8268
7	0.695–0.991	6	3.3707	75,925	4.0423	0.8338
Profile curvature						
1	convex	53	29.7752	550,704	29.9515	0.9941
2	flat	73	41.0112	701,471	38.1514	1.0749
3	concave	52	29.2134	586,472	31.8969	0.9158
Plan curvature						
1	convex	37	20.7865	405,715	22.0659	0.9420
2	flat	103	57.8651	1012,136	55.0478	1.0511
3	concave	38	21.3483	420,796	22.8861	0.9328
LULC						
1	barren land	9	5.0561	270,003	14.5077	0.3485
2	agriculture land	127	71.3483	761,606	40.9224	1.7434
3	forest area	11	6.1797	114,155	6.1337	2.5645
4	built-up area	28	15.7303	680,376	36.5578	0.4302
5	water body	3	1.6853	34,954	1.8781	0.8973

The amount of rainfall is the most important cause of flooding in any location. In this research, it can be observed that the last two sub-classes of the rainfall parameter (346.90–371.34 and 325.24–346.90 mm) occurred in our study area; for these, the FR values were both greater than 1. Conversely, FR values are less than 1 when the rainfall amounts are below 325.24 mm (Table 2). Flood severities decrease when further

away from a river, while the chance of flooding increases in those regions that are close to a river's edge. As a result, the river proximity factor (Fig. 7) (or the distance from a main river, which is an important metric) was generated and reclassified into six classes (Table 2). Distances from a river that are within a range of 2,000 to 5,000 m (and above) have lower probabilities of flooding, as they show FR values that are less than 1; however, distances of 500 to less than 2,000 m have the greatest FR values (3.39 and 2.53, respectively), thus indicating the most severe flood-event potential.

As mentioned, the in methodology section, SPI is a flood-conditioning element that is frequently utilized; it calculates a runoff's erosive potential and ensures terrain stability [13, 46]. For the current research, SPI was calculated and reclassified into five sub-classes (Table 2). SPI sub-classes less than 1 and 4 through 12 show the highest FR values (which leads to higher probabilities of flooding), whereas the remaining sub-classes show FR values that are lower than 1 (which means low probabilities of flooding). The SPI map of the study area is shown in Figure 8.

The TWI factor is one of the most essential aspects of future-flood prediction; this factor was reclassified into six sub-classes (Fig. 10). The study area's north-center portion observed the highest level of TWI; greater TWI scores indicate greater likelihoods of flooding in an area [33]. High FR values (>1.75) can be observed in Classes 8.83 through 21.04, and low FR values can be observed in Classes 2.16 through 7.12 (Table 2). Another key contributing variable for flood events is the topographic roughness index (TRI); this is determined by a study basin's local topography. For the present study, TRI was calculated and reclassified into seven sub-classes (Fig. 9); lower TRI values indicate higher flood probabilities. The TRI sub-classes of 0.009–0.271 and 0.272–0.367 show the highest FR values (1.53 and 1.41), which lead to higher probabilities of flooding.

According to the FR analysis (the correlation among the flood area and the plan and profile curvatures), the highest FR values came in flat shapes (1.07 and 1.05), followed by convex shapes (0.99 and 0.94); these covered more than 50% of the study region (hence, the above-mentioned profile and plan-curvature shapes had the highest flooding likelihoods). A surface run-off is retained for longer by a flat shape – especially during heavy rainfalls; as a result, it is more prone to floods as compared to the other shapes. The LULC for a region can be useful in detecting flood-prone areas [15]. In the current investigation, high FR values could be observed in the forest and agricultural classes (2.56 and 1.74, respectively) (Table 2). These findings confirmed the notion that exposed agriculture areas are especially susceptible to flooding.

4.1. Flood-susceptibility Mapping

After producing separate layers of the ten conditioning factors and computing their FR values, all of the layers were integrated to create the final flood-susceptibility map of the study area by using an overlapping procedure in the ArcGIS. The resulting flood map was classified into four susceptibility classes: low, medium, high, and very high (Fig. 13).

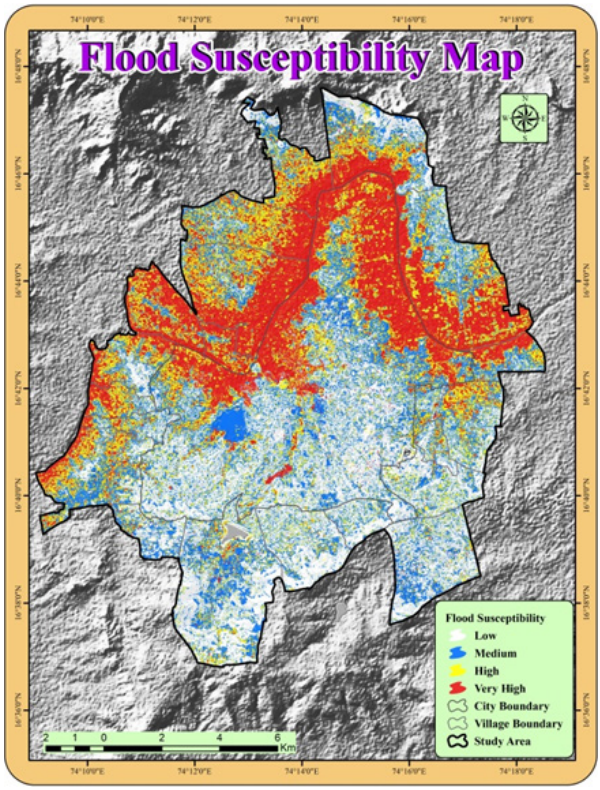

Fig. 13. Flood-susceptibility map

According to the findings, 51.69 km^2 of land (27.83%) were classified as having low flood susceptibilities. This low-flood-susceptibility region could largely be found in the higher-altitude regions (which are shown in the southern side of the research area in Figure 13). A total of 46.23 km^2 (24.89%) of the land was classified as medium susceptibility (which is shown as blue in Figure 13). The results showed that around 39.34 and 48.43 km^2 of land (21.48 and 26.08%, respectively) were segmented as the high- to very-high-susceptibility classes (Table 3); these classes were largely concentrated in the research area's middle north area (shown as yellow and red, respectively, in Figure 13). These classes were characterized by low elevations and low slope gradients, were closer to the main river, featured higher rainfall potentialities, etc. (which are the essential flood-susceptibility-conditioning factors).

Once a model has been created, it is not scientific to use the model for administrative objectives without first validating its correctness and reliability [54]. As a result, it is important to examine the validity of the flood-susceptibility-analysis' accuracy and success rate [55]. The ROC curve was utilized to assess the flood-susceptibility map in the research area. This ROC curve method [38, 53] is a fundamental and universal strategy that uses scientific concepts to appropriately analyze a test.

Table 3. Flood-susceptibility classes

Sr. no.	Flood susceptibility class	Area [km^2]	Area [%]
1	Low	51.69	27.83
2	Medium	46.23	24.89
3	High	39.34	21.18
4	Very high	48.43	26.08

The false positive rate is shown on the x-axis in the ROC curve, while the real positive rate is shown on the y-axis. The area under curve (AUC) is used to verify the accuracy of any model's forecast. This ROC curve method (38, 53) is really a fundamental and universal strategy that uses scientific concepts to appropriately analyze a test on the AUC values: if the value is less than 0.5, then the model is not good for flood mapping; if the value is greater than 0.75, then the model is quite good for flood mapping [38, 56, 57]. Figure 14 depicts the ROC curve for the FR models. Figure 14 clearly indicates that the AUC for the FR model's flood-susceptibility mapping is around 0.878, which corresponds to a prediction accuracy of 87.8%. It is simple to see that the model that was used to create the flood-susceptibility mapping for this research area was correct and acceptable for predicting flood patterns. As a result, the FR model can be considered to be a very valuable tool for flood-susceptibility mapping.

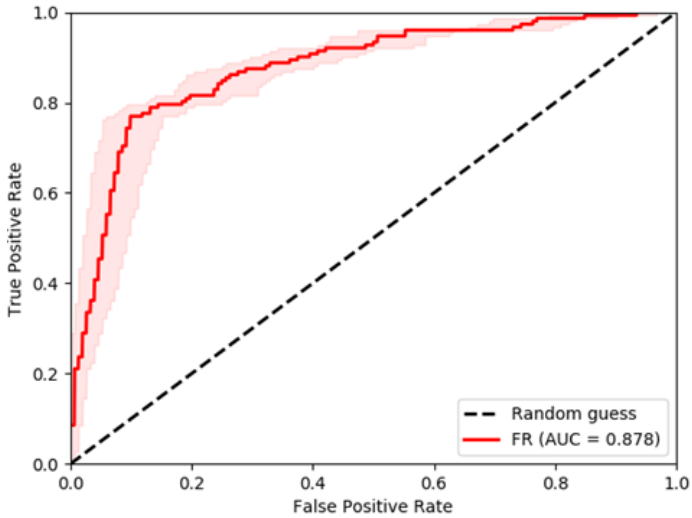

Fig. 14. ROC curve

5. Conclusion

Floods are now regarded as the most devastating calamity on the planet amid a variety of geo-environmental hazards and disasters. Flood-susceptibility mapping is essential for reducing damaging floods by implementing real solutions. Such flood-susceptibility data of this nature is a useful asset for policymakers while implementing accurate land use in flood-prone locations. In this research, the FR model was employed to examine the flood-susceptibility zone. Ten flood conditioning parameters were generated from geospatial data and utilized as inputs in the FR model to map flood-susceptible areas: slope, elevation, rainfall, river proximity, SPI, TWI, TRI, profile and plan curvatures, and LULC. A simple random-sampling method was utilized to choose 70% of the total number of flood points for the FR model and 30% for verification purposes. The finalized flood-susceptibility map was divided into four categories: low, moderate, high, and very high susceptibility classes. In the study area at the lower portion near the river, high- and very-high-susceptibility zones were identified (with 21.18 and 26.08% of the lands, respectively). The ROC curve was generated to validate the flood-susceptibility map in the research area; through this curve, the AUC value was calculated (which showed the prediction accuracy and success rate). The AUC value for the FR model's flood-susceptibility mapping was around 0.878, which corresponded to a prediction accuracy of 87.8%. It is simple to see that the model that was used to create the flood-susceptibility mapping for this research area was correct and acceptable for predicting flood patterns. Thus, the accuracy of the predictor variables can have a substantial impact on flood-susceptibility mapping, as the model's performance improves as the standard levels of the variables rise. This FR model can be applied to other geographic area in order to develop a flood-susceptibility map that will benefit future flood-management planners and decision-makers.

Funding

This research received no specific grant from any funding agency in the public, commercial, or not-for-profit sectors.

CRediT Author Contribution

S. K. P.: conceptualization, data curation, formal analysis, investigation, methodology, resources, writing – original draft, writing – review & editing.

S. S. P.: supervision, validation, writing – review & editing.

Declaration of Competing Interests

The authors declare that they have no known competing financial interests or personal relationships that could have appeared to influence the work reported in this paper.

Use of Generative AI and AI-assisted Technologies

No generative AI or AI-assisted technologies were employed in the preparation of this manuscript.

Acknowledgement

The authors would like to thanks to the Head Department of Geography at Shivaji University Kolhapur for their valuable support and for the use of their equipment and facility. we would also like to thank NRSC for providing the essential data for this study.

References

[1] Du J., Fang J., Xu W., Shi P.: *Analysis of dry/wet conditions using the standardized precipitation index and its potential usefulness for drought/flood monitoring in Hunan Province China.* Stochastic Environmental Research and Risk Assessment, vol. 27(2), 2013, pp. 377–387. https://doi.org/10.1007/s00477-012-0589-6.

[2] Tehrany M.S., Shabani F., Jebur M.N., Hong H., Chen W., Xie X.: *GIS-based spatial prediction of flood prone areas using standalone frequency ratio, logistic regression, weight of evidence and their ensemble techniques*. Geomatics, Natural Hazards and Risk, vol. 8(2), 2017, pp. 1538–1561. https://doi.org/10.1080/19475705.2017.1362038.

[3] Mishra K., Sinha R.: *Flood risk assessment in the Kosi megafan using multi-criteria decision analysis: A hydro-geomorphic approach*. Geomorphology, vol. 350, 2020, 106861. https://doi.org/10.1016/j.geomorph.2019.106861.

[4] Prăvălie R., Costache R.: *The vulnerability of the territorial-administrative units to the hydrological phenomena of risk (flash-floods). Case study: The subcarpathian sector of Buzău catchment*. Analele Universității din Oradea. Seria Geografie, vol. 23(1), 2013, pp. 91–98.

[5] Sarkar D., Mondal P.: *Flood vulnerability mapping using frequency ratio (FR) model: A case study on Kulik river basin, Indo-Bangladesh Barind region*. Applied Water Science, vol. 10(1), 2020, 17. https://doi.org/10.1007/s13201-019-1102-x.

[6] Costache R.: *Flash-flood Potential Index mapping using weights of evidence, decision trees models and their novel hybrid integration*. Stochastic Environmental Research and Risk Assessment, vol. 33(7), 2019, pp. 1375–1402. https://doi.org/10.1007/S00477-019-01689-9.

[7] Hirabayashi Y., Mahendran R., Koirala S., Konoshima L., Yamazaki D., Watanabe S., Kana S.: *Global flood risk under climate change.* Nature Climate Change, vol. 3(9), 2013, pp. 816–821. https://doi.org/10.1038/nclimate1911.

[8] Wahlstrom M., Guha-Sapir D.: *The Human Cost of Weather-related Disasters 1995–2015*. Centre for Research on the Epidemiology of Disasters (CRED) and United Nations Office for Disaster Risk Reduction (UNISDR), Geneva, Switzerland.

[9] Gupta S., Javed A., Dutt D.: *Economics of flood protection in India.* Natural Hazards, vol. 28(1), 2003, pp. 199–210. https://doi.org/10.1023/A:1021142404009.

[10] Singh O., Kumar M.: *Flood events, fatalities and damages in India from 1978 to 2006.* Natural Hazards, vol. 69(3), 2013, pp. 1815–1834. https://doi.org/10.1007/s11069-013-0781-0.

[11] Singh O., Kumar M.: *Flood occurrences, damages, and management challenges in India: A geographical perspective*. Arabian Journal of Geosciences, vol. 10(5), 2017, 102. https://doi.org/10.1007/s12517-017-2895-2.

[12] Cloke H.L., Pappenberger F.: *Ensemble flood forecasting: A review.* Journal of Hydrology, vol. 375(3–4), 2009, pp. 613–626. https://doi.org/10.1016/j.jhydrol.2009.06.005.

[13] Khosravi K., Pradhan B., Pirasteh S., Jebur M.N., Tehrany M.S.: *Flood susceptibility mapping using a novel ensemble weights-of-evidence and support vector machine models in GIS*. Journal of Hydrology, vol. 534, 2016, pp. 173–188. https://doi.org/10.1016/j.jhydrol.2014.03.008.

[14] Kia M.B., Pirasteh S., Pradhan B., Mahmud A.R., Sulaiman W.N.A., Moradi A.: *An artificial neural network model for flood simulation using GIS: Johor River Basin Malaysia.* Environmental Earth Sciences, vol. 67(1), 2012, pp. 251–264. https://doi.org/10.1007/s12665-011-1504-z.

[15] Samanta R.K., Bhunla G.S., Shit P.K., Pourghasemi H.R.: *Flood susceptibility mapping using geospatial frequency ratio technique: A case study of Subarnarekha River Basin. India.* Modeling Earth Systems and Environment, vol. 4(11), 2018, pp. 395–408. https://doi.org/10.1007/s40808-018-0427-z.

[16] Alexander K., Hettiarachchi S., Ou Y., Sharma A.: *Can integrated green spaces and storage facilities absorb the increased risk of flooding due to climate change in developed urban environments?.* Journal of Hydrology, vol. 579, 2019, pp. 124–201. https://doi.org/10.1016/j.jhydrol.2019.124201.

[17] Bubeck P., Thieken A.H.: *What helps people recover from floods? Insights from a survey among flood-affected residents in Germany.* Regional Environmental Change, vol. 18(1), 2018, pp. 287–296. https://doi.org/10.1007/s10113-017-1200-y.

[18] Huang K., Li X., Liu X., Seto K.C.: *Projecting global urban land expansion and heat island intensification through 2050*. Environmental Research Letters, vol. 14(11), 2019, 114037. https://doi.org/10.1088/1748-9326/ab4b71.

[19] Jahandideh-Tehrani M., Zhang H., Helfer F., Yu Y.: *Review of climate change impacts on predicted river streamflow in tropical rivers.* Environmental Monitoring and Assessment, vol. 191(12), 2019, 752. https://doi.org/10.1007/s10661-019-7841-1.

[20] Serraj R., Pingali P.: *Agriculture & Food Systems to 2050: Global Trends, Challenges and Opportunities*. World Scientific Series in Grand Public Policy Challenges of the 21st Century, vol. 2, World Scientific, Singapore 2019. https://doi.org/10.1142/11212.

[21] Su J., Lü H., Zhu Y., Cui Y., Wang X.: *Evaluating the hydrological utility of latest IMERG products over the Upper Huaihe River Basin, China.* Atmospheric Research, vol. 225(1), 2019, pp. 17–29. https://doi.org/10.1016/j.atmosres.2019.03.025.

[22] Cao Q., Mehran A., Ralph F.M., Lettenmaier D.P.: *The role of hydrological initial conditions on atmospheric river floods in the Russian River basin*. Journal of Hydrometeorology, vol. 20(8), 2019, pp. 1667–1686. https://doi.org/10.1175/JHM-D-19-0030.1.

[23] Ali S.A., Khatun R., Ahmad A., Ahmad A.N.: *Application of GIS-based analytic hierarchy process and frequency ratio model to flood vulnerable mapping and risk area estimation at Sundarban region, India*. Modeling Earth System and Environment, vol. 5(3), 2019, pp. 1083–1102. https://doi.org/10.1007/s40808-019-00593-z.

[24] Moel H.D., Vliet M.V., Aerts J.C.J.H.: *Evaluating the effect of flood damage-reducing measures: A case study of the unbanked area of Rotterdam, the Netherlands.* Regional Environmental Change, vol. 14(3), 2014, pp. 895–908. https://doi.org/10.1007/s10113-013-0420-z.

[25] Ebodé V.B., Onguéné R., Braun J.J.: *Flood susceptibility analysis in the Tongo Bassa watershed through the Frequency Ratio Model*. Hydrology Research, vol. 55(4), 2023, pp. 484–497. https://doi.org/10.2166/nh.2024.152.

[26] Ebodé V.B.: *Hydrological variability and flood risk in a forest watershed undergoing accelerated urbanization*. Water Supply, vol. 27(12), 2022, pp. 8778–8794. https://doi.org/10.2166/ws.2022.398.

[27] Haq M., Akhtar M., Muhammad S., Paras S., Rahmatullah J.: *Techniques of Remote Sensing and GIS for flood monitoring and damage assessment: A case study of Sindh province, Pakistan*. The Egyptian Journal of Remote Sensing and Space Science, vol. 15(2), 2012, pp. 135–141. https://doi.org/10.1016/j.ejrs.2012.07.002.

[28] Tehrany M.S., Pradhan B., Juber M.N.: *Flood susceptibility analysis and its verification using a novel ensemble support vector machine and frequency ratio method*. Stochastic Environmental Research and Risk Assessment, vol. 29(4), 2015, pp. 1149–1165. https://doi.org/10.1007/s00477-015-1021-9.

[29] Dhote P.R., Joshi Y., Rajib A., Thakur P.K., Nikam B.R., Aggarwal S.P.: *Evaluating topography-based approaches for fast floodplain mapping in data-scarce complex-terrain regions: Findings from a Himalayan basin.* Journal of Hydrology, vol. 620(part A), 2023, 129309. https://doi.org/10.1016/j.jhydrol.2023.129309.

[30] Lee M.J., Kang J.E., Jeon S.: *Application of frequency ratio model and validation for predictive flooded area susceptibility mapping using GIS*. [in:] *IGARSS 2012: IEEE International Geoscience and Remote Sensing Symposium: Remote Sensing for a Dynamic Earth: Proceedings: July 22–27, 2012, Munich, Germany*, IEEE, Piscataway 2012, pp. 895–898. https://doi.org/10.1109/IGARSS.2012.6351414.

[31] Jebur M.N., Pradhan B., Tehrany M.S.: *Optimization of landslide conditioning factors using very high-resolution airborne laser scanning (LiDAR) data at catchment scale*. Remote Sensing and Environment, vol. 152, 2014, pp. 150–165. https://doi.org/10.1016/j.rse.2014.05.013.

[32] Tien Bui D., Pradhan B., Lofman O., Revhaug I., Dick O.B:. *Spatial prediction of landslide hazards in Hoa Binhprovince (Vietnam): A comparative assessment of the efficacy of evidential belief functions and fuzzy logic models*. Catena, vol. 96, 2012, pp. 28–40. https://doi.org/10.1016/j.catena.2012.04.001.

[33] Rahmati O., Pourghasemi H.R., Zeinivand H.: *Flood susceptibility mapping using frequency ratio and weights-of-evidence models in the Golastan Province, Iran*. Geocarto International, vol. 31(1), 2016, pp. 42–70. https://doi.org/10.1080/10106049.2015.1041559.

[34] Sujatha E.R., Rajamanickam V., Kumaravel P., Saranathan E.: *Landslide susceptibility analysis using probabilistic likelihood ratio model – a geospatial-based study*. Arabian Journal of Geosciences, vol. 6(2), 2013, pp. 429–440. https://doi.org/10.1007/s12517-011-0356-x.

[35] Tehrany M.S., Lee M.J., Pradhan B., Jebur M.N., Lee S.: *Flood susceptibility mapping using integrated bivariate and multivariate statistical models*. Environmental Earth Science, vol. 72(10), 2014, pp. 4001–4015. https://doi.org/10.1007/s12665-014-3289-3.

[36] Liao X., Carin L.: *Migratory logistic regression for learning concept drift between two data sets with application to UXO sensing*. IEEE Transactions on Geoscience and Remote Sensing, vol. 47(5), 2009, pp. 1454–1466. https://doi.org/10.1109/TGRS.2008.2005268.

[37] Manandhar B.: *Flood plain analysis and risk assessment of Lothar Khola*. Tribhuvan University, Phokara, Nepal, 2010 [MSc thesis].

[38] Pradhan B., Lee S.: *Delineation of landslide hazard areas on Penang Island, Malaysia, by using frequency ratio, logistic regression, and artificial neural network models*. Environmental Earth Sciences, vol. 60(5), 2010, pp. 1037–1054. https://doi.org/10.1007/s12665-009-0245-8.

[39] Pourghasemi H.R., Beheshtirad M.: *Assessment of a data-driven evidential belief function model and GIS for groundwater potential mapping in the Koohrang Watershed, Iran.* Geocarto International, vol. 30(6), 2014, pp. 662–685. https://doi.org/10.1080/10106049.2014.966161.

[40] Tunusluoglu M., Gokceoglu C., Nefeslioglu H., Sonmez H.: *Extraction of potential debris source areas by logistic regression technique: A case study from Barla, Besparmak and Kapi mountains (NW Taurids, Turkey).* Environmental Earth Sciences, vol. 54(1), 2008, pp. 9–22. https://doi.org/10.1007/s00254-007-0788-5.

[41] Samanta S., Pal D.K., Lohar D., Pal B.: *Interpolation of climate variables and temperature modeling.* Theoretical and Applied Climatolgy, vol. 107(1), 2012, pp. 35–45. https://doi.org/10.1007/s00704-011-0455-3.

[42] Youssef A.M., Pradhan B., Hassan A.M.: *Flash flood risk estimation along the St. Katherine road, southern Sinai, Egypt using GIS based morphometry and satellite imagery*. Environmental Earth Sciences, vol. 62(3), 2011, pp. 611–623. https://doi.org/10.1007/s12665-010-0551-1.

[43] Ebodé V.B., Ngono Onana J.Y., Dzana J.G., Amougou J.A., Batha A., Boyomo T., Ndjela Mbeih G.: *Availability of the current and future water resources in Equatorial Central Africa: Case of the Nyong forest catchment in Cameroon*. Environmental Monitoring and Assessment, vol. 196(3), 2024, 298. https://doi.org/10.1007/s10661-024-12471-y.

[44] Tehrany M.S., Pradhan B., Jebur M.N.: *Spatial prediction of flood susceptible areas using rule based decision tree (DT) and a novel ensemble bivariate and multivariate statistical models in GIS*. Journal of Hydrology, vol. 504, 2013, pp. 69–79. https://doi.org/10.1016/j.jhydrol.2013.09.034.

[45] Lee S., Kim J.C., Jung H.S., Lee M.J., Lee S.: *Spatial prediction of flood susceptibility using random-forest and boosted-tree models in Seoul metropolitan city, Korea*. Geomatics, Natural Hazards and Risk, vol. 8(2), 2017, pp. 1185–1203. https://doi.org/10.1080/19475705.2017.1308971.

[46] Tehrany M.S., Jones S., Shabani F.: *Identifying the essential flood conditioning factors for flood prone area mapping using machine learning techniques.* Catena, vol. 175, 2019, pp. 174–192. https://doi.org/10.1016/j.catena.2018.12.011.

[47] Casas A., Lane S.N., Yu D., Benito G.: *A method for parameterising roughness and topographic sub-grid scale effects in hydraulic modelling from LiDAR data*. Hydrology and Earth System Sciences, vol. 14(8), 2010, pp. 1567–1579. https://doi.org/10.5194/hess-14-1567-2010.

[48] Moore I.D., Grayson R.B., Ladson A.R.: *Digital terrain modelling: A review of hydrological, geomorphological, and biological applications*. Hydrological Processes, vol. 5(1), 1991, pp. 3–30. https://doi.org/10.1002/hyp.3360050103.

[49] Haghizadeh A., Siahkamari S., Haghiabi A.H., Rahmati O.: *Forecasting flood-prone areas using Shannon's entropy model*. Journal of Earth System Science, vol. 126(3), 2017, 39. https://doi.org/10.1007/s12040-017-0819-x.

[50] Hong H., Tsnagaratos P., Ilia J., Liu J., Zhu A., Chen W.: *Application of fuzzy weight of evidence and data mining techniques in construction of flood susceptibility map of Poyang County, China*. Science of Total Environment, vol. 625, 2017, pp. 575–588. https://doi.org/10.1016/j.scitotenv.2017.12.256.

[51] Lee S., Talib J.A.: *Probabilistic landslide susceptibility and factor effect analysis*. Environmental Geology, vol. 47(7), 2005, pp. 982–990. https://doi.org/10.1007/s00254-005-1228-z.

[52] Pradhan B., Buchroithner M.F.: *Comparison and validation of landslide susceptibility maps using an artificial neural network model for three test areas in Malaysia*. Environmental & Engineering Geoscience, vol. 16(2), 2010, pp. 107–126. https://doi.org/10.2113/gseegeosci.16.2.107.

[53] Pourghasemi H.R., Pradhan B., Gokceoglu C.: *Remote sensing data derived parameters and its use in landslide susceptibility assessment using Shannon's entropy and GIS*. Applied Mechanics and Materials, vol. 225, 2012, pp. 486–491. https://doi.org/10.4028/www.scientific.net/AMM.225.486.

[54] Chung C.F., Fabbri A.G.: *Validation of spatial prediction models for landslide hazard mapping*. Natural Hazards, vol. 30(3), 2003, pp. 451–472. https://doi.org/10.1023/B:NHAZ.0000007172.62651.2b.

[55] Tien Bui D., Pradhan B., Lofman O., Revhaug I., Dick O.B.: *Landslide susceptibility mapping at Hoa Binh province (Vietnam) using an adaptive neuro-fuzzy inference system and GIS*. Computers & Geosciences, vol. 45, 2012, pp. 199–211. https://doi.org/10.1016/j.cageo.2011.10.031.

[56] Saha S.: *Groundwater potential mapping using analytical hierarchical process: A study on Md. Bazar Block of Birbhum District, West Bengal*. Spatial Information Research, vol. 25(4), 2017, pp. 615–626. https://doi.org/10.1007/s41324-017-0127-1.

[57] Ozdemir A., Altural T.: *A comparative study of frequency ratio, weights of evidence and logistic regression methods for landslide susceptibility mapping: Sultan Mountains, SW Turkey*. Journal of Asian Earth Sciences, vol. 64(5), 2013, pp. 180–197. https://doi.org/10.1016/j.jseaes.2012.12.014.